Finite Element Analysis of Anisotropic Structures at Large Inelastic Deformations

Bernhard Eidel, Friedrich Gruttmann

Institut für Werkstoffe und Mechanik im Bauwesen, FB 13
Technische Universität Darmstadt
Alexanderstraße 7, 64283 Darmstadt, Germany

Contents

Report/Preprint No. 4

to appear in: *Springer Lecture Notes in Mechanics*

August, 15, 2002

Finite Element Analysis of Anisotropic Structures at Large Inelastic Deformations

Bernhard Eidel and Friedrich Gruttmann

Institut für Werkstoffe und Mechanik im Bauwesen, TU Darmstadt, Germany

Abstract. A constitutive model for orthotropic elastoplasticity at finite plastic strains is discussed and basic concepts of its numerical implementation are presented. The essential features are the multiplicative decomposition of the deformation gradient in elastic and inelastic parts, the definition of a convex elastic domain in stress space and a representation of the constitutive equations related to the intermediate configuration. The elastic free energy function and the yield function are formulated in an invariant setting by means of the introduction of structural tensors reflecting the privileged directions of the material. The model accounts for kinematic and isotropic hardening. The associative flow rule is integrated using the so–called exponential map which preserves exactly the plastic incompressibility condition. The constitutive equations are implemented in a brick type shell element. Due to special interpolation techniques the element is able to predict a locking-free deformation behaviour even for very thin structures. Representative numerical simulations demonstrate the suitability of the proposed formulations.

1 Introduction

Many elastoplastic materials exhibit anisotropic behavior due to their textured or generally orientation dependent structure. The response of anisotropic materials can be described with scalar-valued functions in terms of several tensor variables, usual deformation or stress tensors and additional structural tensors, which reflect the symmetries of the considered material. Based on representation theorems for tensor functions the general forms can be derived and the type and minimal number of the scalar variables entering the constitutive equations can be given. These forms are automatically invariant under coordinate transformations of elements of the material symmetry group. For an introduction to the invariant formulation of anisotropic constitutive equations based on the concept of structural tensors and their representations as isotropic tensor functions see Betten [5], Boehler [7], Spencer [37].

For a state-of-the-art review of the recent progress in the theory and numerics of anisotropic materials at finite strains we refer to the papers published in a special issue of the International Journal of Solids and Structures Vol. 38 (2001), EUROMECH Colloquium 394, and the references therein. In the following we mention some contributions in the field of anisotropic elastoplasticity being aware that this short overview cannot be complete. A yield criterion which describes the plastic flow of orthotropic metals has been first

proposed in the pioneering work of Hill [18]. A numerical study on integration algorithms for Hill's model at small strains is given in De Borst & Feenstra [8]. In [24] Miehe presented a constitutive framework for the formulation of large strain anisotropic elastoplasticity based on the notion of a plastic metric. In the paper of Xiao et al. [42] a consistent Eulerian type constitutive elastoplasticity theory including isotropic and kinematic hardening was developed, which combines the additive and multiplicative decomposition of the stretch tensor and the deformation gradient. Papadopoulos & Lu [27] proposed an anisotropic elastoplasticity model using a family of generalized stress-strain measures. A thermodynamically consistent theory of plastic anisotropy at large deformations taking into account the postulate of Il'iushin is proposed by Tsakmakis [39]. To describe the rotation of the underlying substructure evolution equations for the symmetry axes are formulated. In the context of Il'iushin's postulate see also Besdo [2], where constitutive equations of plasticity theory are formulated in strain space.
For some results concerning the mathematical treatment of finite multiplicative elastoplasticity see Neff [25]. A formulation of multiplicative finite strain elastoplasticity within the framework of generalized standard media was proposed by Hackl in [17].

The essential features of this paper are summarized as follows:
(i) In our formulation the multiplicative decomposition of the deformation gradient in elastic and inelastic parts is assumed to apply. A yield function, related to the intermediate configuration is expressed in terms of the so called Mandel stress tensor and a back stress tensor for kinematic hardening.
(ii) The constitutive equations for elastoplastic orthotropy are formulated in an invariant setting. So-called structural tensors describe the symmetries of the material in the elastic free energy function and the yield condition. The latter is expressed in terms of the invariants of the deviatoric part of the relative Mandel stresses and of the structural tensors.
(iii) The set of constitutive equations is solved by applying a general return method based on an operator split into an elastic predictor and a following corrector step. Plastic incompressibility is fulfilled exactly by means of the exponential map.
(iv) For finite element simulations of engineering problems in structural mechanics we use a formulation of a brick-type shell element, documented in Klinkel [20], that overcomes artificial stiffening effects, called *locking*, by means of special interpolation techniques. Thus, the element is well suited for the numerical analysis of thin structures.
(v) We investigate four representative numerical examples: The necking of a circular bar and the punching of a conical shell, both for elastoplastic isotropy; for orthotropic material behaviour we consider the drawing of a circular blank and the bending of a circular plate.
Earlier versions of the authors work on anisotropic elastoplasticity and further numerical results can be found in [11] and [15].

2 Kinematics and Constitutive Framework

The considered body in the reference configuration is denoted by $\mathcal{B} \subset \mathbb{R}^3$. It is parametrized in $\mathbf{X}$ and the current configuration $\mathcal{S} \subset \mathbb{R}^3$ is parametrized in $\mathbf{x}$. The nonlinear deformation map $\boldsymbol{\varphi}_t : \mathcal{B} \to \mathcal{S}$ at time $t \in R_+$ maps points $\mathbf{X} \in \mathcal{B}$ onto points $\mathbf{x} \in \mathcal{S}$. Hence, the deformation gradient $\mathbf{F}$ is defined by $\mathbf{F}(\mathbf{X}) := \mathrm{Grad}\, \boldsymbol{\varphi}_t(\mathbf{X})$ with the Jacobian $J(\mathbf{X}) := \det \mathbf{F}(\mathbf{X}) > 0$. The index notation of $\mathbf{F}$ is $F^a{}_A := \partial x^a / \partial X^A$. Next, the right Cauchy–Green tensor is introduced by $\mathbf{C} = \mathbf{F}^T\mathbf{F}$ with coefficients $C_{AB} = F^a{}_A F^b{}_B g_{ab}$, where g_{ab} denotes the coefficients of the covariant metric tensor in the current configuration.

2.1 Multiplicative Elastoplasticity

Motivated by a micromechanical view of plastic deformations one postulates a multiplicative decomposition of the deformation gradient

$$\mathbf{F}(\mathbf{X}) = \mathbf{F}^e(\mathbf{X})\, \mathbf{F}^p(\mathbf{X})\,, \tag{1}$$

with the elastic and plastic parts $\mathbf{F}^e$ and $\mathbf{F}^p$, respectively. Equation (1) implies a stress-free intermediate configuration, which is in general not compatible. It is well-known that the decomposition is uniquely determined except for a rigid body rotation superposed on the intermediate configuration. Original references dealing with (1) can be found in the textbook by Lubliner [21]. Furthermore, the plastic incompressibility constraint

$$\det \mathbf{F}^p(\mathbf{X}) = 1 \tag{2}$$

is assumed to hold. The constitutive equations are restricted by the second law of thermodynamics in the form of the Clausius–Duhem-inequality, which reads under the assumption of isothermal deformations with uniform temperature distribution

$$\mathcal{D} = \mathbf{S} : \dot{\mathbf{E}} - \dot{\psi} \geq 0\,. \tag{3}$$

In this local form the dissipation $\mathcal{D}$ denotes the difference between the stress power and the rate of the free energy per unit volume in the reference configuration. $\mathbf{S}$ and $\dot{\mathbf{E}}$ are the Second Piola–Kirchhoff stress tensor and the material time derivative of the Green–Lagrangian strain tensor $\mathbf{E} = \frac{1}{2}(\mathbf{C} - \mathbf{1})$, respectively. Here and in the following $\mathbf{1}$ denotes the second order unit tensor. Introducing the free energy $\psi = \psi(\mathbf{C}^e, \boldsymbol{\chi})$ as a function of the elastic right Cauchy–Green tensor $\mathbf{C}^e := \mathbf{F}^{e\,T}\,\mathbf{F}^e$ and the internal variables $\boldsymbol{\chi}$ – considered to be in general a set of tensors and scalars and represented as a vector – the associated rate is given by

$$\dot{\psi} = \frac{\partial \psi}{\partial \mathbf{C}^e} : \dot{\mathbf{C}}_e + \frac{\partial \psi}{\partial \boldsymbol{\chi}} \cdot \dot{\boldsymbol{\chi}}\,. \tag{4}$$

The strain rate $\dot{\mathbf{E}} = \frac{1}{2}\dot{\mathbf{C}}$ is derived by considering the multiplicative decomposition (1). One obtains, see e.g. [21],

$$\dot{\mathbf{C}} = \mathbf{F}^{p\,T}\,[\dot{\mathbf{C}}^e + 2(\mathbf{C}^e\,\mathbf{L}^p)_s]\,\mathbf{F}^p \quad \text{with} \quad \mathbf{L}^p = \dot{\mathbf{F}}^p\mathbf{F}^{p\,-1}\,, \tag{5}$$

where $\mathbf{L}^p$ denotes the plastic velocity gradient and $()_s$ describes the symmetric part of a tensor. Since inequality (3), considering (4) and (5), must hold for all admissible processes in the material, standard arguments in rational thermodynamics with internal state variables yield the constitutive equations

$$\hat{\mathbf{S}} = 2\frac{\partial\psi}{\partial\mathbf{C}^e} \quad , \quad \boldsymbol{\Xi} = \frac{\partial\psi}{\partial\boldsymbol{\chi}}\,. \tag{6}$$

Here, $\hat{\mathbf{S}} = \mathbf{F}^p\,\mathbf{S}\,\mathbf{F}^{p\,T}$ denotes the Second Piola–Kirchhoff stress tensor relative to the intermediate configuration and $\boldsymbol{\Xi}$ the internal stress vector conjugate to $\boldsymbol{\chi}$. Furthermore, one obtains the reduced local dissipation inequality

$$\mathcal{D} = \boldsymbol{\Sigma} : \mathbf{L}^p - \boldsymbol{\Xi}\cdot\dot{\boldsymbol{\chi}} \geq 0\,, \tag{7}$$

where we call $\boldsymbol{\Sigma} := \mathbf{C}^e\,\hat{\mathbf{S}}$ the Mandel stress tensor, which for anisotropic elasticity is in general nonsymmetric.

The evolution equations for the inelastic strain tensors can be derived by using the principle of maximum plastic dissipation. If the elastic domain E defined by the yield function $\Phi \leq 0$ is convex, a standard result in convex analysis shows, that, along with the loading-unloading conditions, the following normality rules for the rate equations of inelastic strains must hold

$$\mathbf{L}^p = \lambda\frac{\partial\Phi}{\partial\boldsymbol{\Sigma}} \quad , \qquad \dot{\boldsymbol{\chi}} = -\lambda\frac{\partial\Phi}{\partial\boldsymbol{\Xi}}\,. \tag{8}$$

In the following we specify the vector $\boldsymbol{\Xi}$ by introducing the scalar, stress like hardening variable ξ and the back stress tensor $\hat{\boldsymbol{\beta}}$ for isotropic and kinematic hardening, respectively. Furthermore, we assume that the free energy function is additively decoupled in an elastic part ψ^e, a plastic part $\psi^{p,iso}$ due to isotropic hardening and $\psi^{p,kin}$ due to kinematic hardening of Melan–Prager type. The yield criterion Φ is formulated in terms of the relative stresses $\hat{\boldsymbol{\sigma}} := \boldsymbol{\Sigma} - \hat{\boldsymbol{\beta}}$ and the isotropic hardening stress ξ. According to (8) the evolution of the plastic deformation gradient $\mathbf{F}^p$ and of the internal variables $\boldsymbol{\chi}$ are given with Φ as a plastic potential. Here, $\boldsymbol{\chi}$ contains the tensor valued $\boldsymbol{\alpha}$, conjugate to the back stress $\hat{\boldsymbol{\beta}}$ as well as the scalar valued equivalent plastic strain e^p, conjugate to ξ.

2.2 Isotropic Tensor Functions for the Representation of Anisotropic Material Response

In case of anisotropy we introduce a material symmetry group $\mathcal{G}_k$ characterizing the anisotropy class of the material. $\mathcal{G}_k$ is defined with respect to

the reference configuration, and we assume that it remains unchanged during plastic deformations. The elements of $\mathcal{G}_k$ are denoted by the unimodular tensors ${}^i\mathbf{Q}|i = 1, ..., n$. Here, the concept of material symmetry will be formulated for an orthotropic elasticity law, which is related to the intermediate configuration and therefore is expressed in terms of the elastic Green strain tensor $\hat{\mathbf{E}}^e = (\mathbf{C}^e - \mathbf{1})/2$. Based on our assumption this concept requires that the elastic material response must be invariant under transformations on the intermediate configuration with elements of the symmetry group $\mathcal{G}_k$

$$\hat{\psi}^e(\mathbf{Q}^T\hat{\mathbf{E}}^e\mathbf{Q}) = \hat{\psi}^e(\hat{\mathbf{E}}^e) \quad \forall\, \mathbf{Q} \in \mathcal{G}_k, \hat{\mathbf{E}}^e \,. \tag{9}$$

We call the function ψ^e a $\mathcal{G}_k$-invariant function. Having only solid materials in mind we set $\mathcal{G}_k \subset \mathrm{SO}(3)$. Based on the mapping $\hat{\mathbf{X}} \to \mathbf{Q}^T\hat{\mathbf{X}}$, applied to the intermediate configuration $\hat{\mathbf{X}}$, for arbitrary rotation tensors $\mathbf{Q} \in \mathrm{SO}(3)$ we have, in view of a coordinate free representation, to fulfill the transformation rule $\mathbf{Q}^T\hat{\mathbf{S}}(\hat{\mathbf{E}}^e, \bullet)\mathbf{Q} = \hat{\mathbf{S}}(\mathbf{Q}^T\hat{\mathbf{E}}^e\mathbf{Q}, \bar{\bullet})\ \ \forall \mathbf{Q} \in \mathrm{SO}(3)$, where $(\bullet)$ denotes additional tensor arguments, also subject to $\mathcal{G}_k$ and $(\bar{\bullet})$ represents the $\mathbf{Q}$-transformed tensors. In order to construct an isotropic tensor function for the anisotropic constitutive behavior, the $\mathcal{G}_k$-invariant function must be extended in a manner, that it becomes invariant under the special orthogonal group; this is done by the introduction of the so-called structural tensors reflecting the material symmetries. Recall here, that a second order tensor $\mathbf{M}$ is a structural tensor of an anisotropic material characterized by a symmetry group $\mathcal{G}_k$ if $\mathbf{Q}^T\mathbf{M}\mathbf{Q} = \mathbf{M}$ for all $\mathbf{Q} \in \mathcal{G}_k$. Orthotropic materials can be characterized by three symmetry planes, described by three structural tensors ${}^i\mathbf{M}|i = 1, 2, 3$. Thus, the constitutive equation can be expressed as an isotropic scalar-valued tensor function in the arguments $(\hat{\mathbf{E}}^e, {}^1\mathbf{M}, {}^2\mathbf{M}, {}^3\mathbf{M})$ in the form

$$\hat{\psi}^e(\hat{\mathbf{E}}^e, {}^i\mathbf{M}|_{i=1,2,3}) = \hat{\psi}^e(\mathbf{Q}^T\hat{\mathbf{E}}^e\mathbf{Q}, \mathbf{Q}^T{}^i\mathbf{M}\mathbf{Q}|_{i=1,2,3}) \ \ \forall\, \mathbf{Q} \in \mathrm{SO}(3) \,. \tag{10}$$

which fulfills the above postulated transformation rule for the stresses.

2.3 Orthotropic Elastic Free Energy Function

The material symmetry group of the considered orthotropic material is defined by $\mathcal{G}_o := \{\mathbf{I}; \mathbf{S}_1, \mathbf{S}_2, \mathbf{S}_3\}$, where $\mathbf{S}_1, \mathbf{S}_2, \mathbf{S}_3$ are the reflections with respect to the basis planes $({}^2\mathbf{a}, {}^3\mathbf{a})$, $({}^3\mathbf{a}, {}^1\mathbf{a})$ and $({}^1\mathbf{a}, {}^2\mathbf{a})$, respectively. Here, $({}^1\mathbf{a}, {}^2\mathbf{a}, {}^3\mathbf{a})$ represents an orthonormal privileged frame. Based on this, we obtain for this symmetry group the three structural tensors

$${}^1\mathbf{M} := {}^1\mathbf{a} \otimes {}^1\mathbf{a}, \quad {}^2\mathbf{M} := {}^2\mathbf{a} \otimes {}^2\mathbf{a} \quad \text{and} \quad {}^3\mathbf{M} := {}^3\mathbf{a} \otimes {}^3\mathbf{a} \,, \tag{11}$$

which represent the orthotropic material symmetry. Due to the fact that the sum of the three structural tensors yields $\sum_{i=1}^{3} {}^i\mathbf{M} = \mathbf{1}$ we may discard ${}^3\mathbf{M}$ from the set of structural tensors (11). The integrity basis is given by

$$\mathcal{P} := \{J_1, ..., J_7\} \,. \tag{12}$$

The invariants J_1, J_2, J_3 are defined by the traces of powers of $\hat{\mathbf{E}}^e$, i.e.,

$$J_1 := \mathrm{tr}\hat{\mathbf{E}}^e \ , \quad J_2 := \mathrm{tr}[(\hat{\mathbf{E}}^e)^2] \ , \quad J_3 := \mathrm{tr}[(\hat{\mathbf{E}}^e)^3] \ . \tag{13}$$

The irreducible mixed invariants are given by

$$\left.\begin{array}{ll} J_4 := \mathrm{tr}[{}^1\mathbf{M}\hat{\mathbf{E}}^e] \ , & J_5 := \mathrm{tr}[{}^1\mathbf{M}(\hat{\mathbf{E}}^e)^2] \\ J_6 := \mathrm{tr}[{}^2\mathbf{M}\hat{\mathbf{E}}^e] \ , & J_7 := \mathrm{tr}[{}^2\mathbf{M}(\hat{\mathbf{E}}^e)^2] \end{array}\right\} \ , \tag{14}$$

see e.g. SPENCER [37]. For ψ^e we assume a quadratic form, viz.,

$$\psi^e = \tfrac{1}{2}\lambda J_1^2 + \mu J_2 + \tfrac{1}{2}\alpha_1 J_4^2 + \tfrac{1}{2}\alpha_2 J_6^2 + 2\alpha_3 J_5 + 2\alpha_4 J_7 + \alpha_5 J_4 J_1 + \alpha_6 J_6 J_1 + \alpha_7 J_4 J_6 \ . \tag{15}$$

For the 2nd Piola–Kirchhoff stresses related to the intermediate configuration we have

$$\left.\begin{array}{l} \hat{\mathbf{S}} = \lambda J_1 \mathbf{1} + 2\mu\hat{\mathbf{E}}^e + \alpha_1 J_4\, {}^1\mathbf{M} + \alpha_2 J_6\, {}^2\mathbf{M} + 2\alpha_3(\hat{\mathbf{E}}^e\, {}^1\mathbf{M} + {}^1\mathbf{M}\hat{\mathbf{E}}^e) \\ \quad +2\alpha_4(\hat{\mathbf{E}}^e\, {}^2\mathbf{M} + {}^2\mathbf{M}\hat{\mathbf{E}}^e) + \alpha_5(J_1\, {}^1\mathbf{M} + J_4\mathbf{1}) \\ \quad +\alpha_6(J_1\, {}^2\mathbf{M} + J_6\mathbf{1}) + \alpha_7(J_4\, {}^2\mathbf{M} + J_6\, {}^1\mathbf{M}) \end{array}\right\} \ . \tag{16}$$

In this special case the second derivative of ψ^e yields the constant fourth-order elasticity tensor

$$\left.\begin{array}{l} \mathbb{C}^e = \lambda\mathbf{1}\otimes\mathbf{1} + 2\mu\mathbb{I} + \alpha_1\, {}^1\mathbf{M}\otimes{}^1\mathbf{M} + \alpha_2\, {}^2\mathbf{M}\otimes{}^2\mathbf{M} \\ \quad +2\alpha_3\mathbb{K}_1 + 2\alpha_4\mathbb{K}_2 + \alpha_5({}^1\mathbf{M}\otimes\mathbf{1} + \mathbf{1}\otimes{}^1\mathbf{M}) \\ \quad +\alpha_6({}^2\mathbf{M}\otimes\mathbf{1} + \mathbf{1}\otimes{}^2\mathbf{M}) + \alpha_7({}^2\mathbf{M}\otimes{}^1\mathbf{M} + {}^1\mathbf{M}\otimes{}^2\mathbf{M}) \end{array}\right\} \tag{17}$$

with $\mathbb{I}_{IJKL} = \delta_{IK}\delta_{JL}$, $\mathbb{K}^1_{IJKL} = \delta_{IK}\,{}^1M_{JL} + \delta_{JL}\,{}^1M_{IK}$ and $\mathbb{K}^2_{IJKL} = \delta_{IK}\,{}^2M_{JL} + \delta_{JL}\,{}^2M_{IK}$. The elasticity parameters $(\lambda, \mu, \alpha_i | i = 1, \ldots, 7)$ can be identified by using the matrix notation

$$\begin{bmatrix} \hat{S}_{11} \\ \hat{S}_{22} \\ \hat{S}_{33} \\ \hat{S}_{12} \\ \hat{S}_{13} \\ \hat{S}_{23} \end{bmatrix} = \begin{bmatrix} \mathbb{C}_{11} & \mathbb{C}_{12} & \mathbb{C}_{13} & 0 & 0 & 0 \\ \mathbb{C}_{12} & \mathbb{C}_{22} & \mathbb{C}_{23} & 0 & 0 & 0 \\ \mathbb{C}_{13} & \mathbb{C}_{23} & \mathbb{C}_{33} & 0 & 0 & 0 \\ 0 & 0 & 0 & \mathbb{C}_{44} & 0 & 0 \\ 0 & 0 & 0 & 0 & \mathbb{C}_{55} & 0 \\ 0 & 0 & 0 & 0 & 0 & \mathbb{C}_{66} \end{bmatrix} \begin{bmatrix} \hat{E}^e_{11} \\ \hat{E}^e_{22} \\ \hat{E}^e_{33} \\ 2\hat{E}^e_{12} \\ 2\hat{E}^e_{13} \\ 2\hat{E}^e_{23} \end{bmatrix} \ , \tag{18}$$

with the elasticity constants $\mathbb{C}_{ij}$. Choosing the preferred directions as ${}^1\mathbf{a} = (1,0,0)^T$ and ${}^2\mathbf{a} = (0,1,0)^T$ we obtain the material parameters

$$\left.\begin{aligned}
\lambda &= \mathbb{C}_{33} + 2(\mathbb{C}_{44} - \mathbb{C}_{55} - \mathbb{C}_{66}) \\
\mu &= \mathbb{C}_{55} + \mathbb{C}_{66} - \mathbb{C}_{44} \\
\alpha_1 &= \mathbb{C}_{11} + \mathbb{C}_{33} - 4\mathbb{C}_{55} - 2\mathbb{C}_{13} \\
\alpha_2 &= \mathbb{C}_{22} + \mathbb{C}_{33} - 4\mathbb{C}_{66} - 2\mathbb{C}_{23} \\
\alpha_3 &= \mathbb{C}_{44} - \mathbb{C}_{66} \\
\alpha_4 &= \mathbb{C}_{44} - \mathbb{C}_{55} \\
\alpha_5 &= \mathbb{C}_{13} - \mathbb{C}_{33} - 2(\mathbb{C}_{44} - \mathbb{C}_{55} - \mathbb{C}_{66}) \\
\alpha_6 &= \mathbb{C}_{23} - \mathbb{C}_{33} - 2(\mathbb{C}_{44} - \mathbb{C}_{55} - \mathbb{C}_{66}) \\
\alpha_7 &= \mathbb{C}_{12} - \mathbb{C}_{13} - \mathbb{C}_{23} + \mathbb{C}_{33} + 2(\mathbb{C}_{44} - \mathbb{C}_{55} - \mathbb{C}_{66})
\end{aligned}\right\} \tag{19}$$

in the invariant setting. In case of isotropy the only remaining constants are λ and μ, which can be directly determined from Young's modulus E and Poisson's ratio ν via $\mu = E/2(1+\nu)$, $\lambda = E\nu/(1+\nu)(1-2\nu)$.

2.4 Orthotropic Yield Criterion

In the following, we consider an orthotropic pressure insensitive yield condition using isotropic tensor functions. It is assumed that Φ depends on the symmetric part of the relative stresses $\hat{\boldsymbol{\sigma}}_s := (\boldsymbol{\Sigma} - \hat{\boldsymbol{\beta}})_s$ only. As a consequence the following relations hold for the plastic velocity gradients

$$\mathbf{L}^p = \mathbf{L}^{p\,T} \;\;,\;\; \mathbf{D}^p := \mathrm{sym}(\mathbf{L}^p) = \mathbf{L}^p \;\;,\;\; \mathbf{W}^p := \mathrm{skew}(\mathbf{L}^p) = \mathbf{0}\,. \tag{20}$$

This assumption and its implications will be discussed below.
The integrity basis in terms of the deviatoric part of the relative stresses $\mathrm{dev}\,\hat{\boldsymbol{\sigma}}_s$ and the structural tensors ${}^1\mathbf{M}$ and ${}^2\mathbf{M}$ is given by

$$\left.\begin{aligned}
I_1 := \mathrm{tr}\,[(\mathrm{dev}\hat{\boldsymbol{\sigma}}_s)^2],\;\; I_2 := \mathrm{tr}\,[{}^1\mathbf{M}(\mathrm{dev}\hat{\boldsymbol{\sigma}}_s)^2],\;\; I_3 := \mathrm{tr}\,[{}^2\mathbf{M}(\mathrm{dev}\hat{\boldsymbol{\sigma}}_s)^2] \\
I_4 := \mathrm{tr}\,[{}^1\mathbf{M}\mathrm{dev}\hat{\boldsymbol{\sigma}}_s],\;\; I_5 := \mathrm{tr}\,[{}^2\mathbf{M}\mathrm{dev}\hat{\boldsymbol{\sigma}}_s],\;\; I_6 := \mathrm{tr}\,[(\mathrm{dev}\hat{\boldsymbol{\sigma}}_s)^3]
\end{aligned}\right\}\,. \tag{21}$$

The orthotropic flow criterion is formulated as an isotropic tensor function

$$\hat{\Phi}(\mathrm{dev}\hat{\boldsymbol{\sigma}}_s, {}^1\mathbf{M}, {}^2\mathbf{M}) = \hat{\Phi}(\mathbf{Q}^T\mathrm{dev}\hat{\boldsymbol{\sigma}}_s\mathbf{Q}, \mathbf{Q}^T\,{}^1\mathbf{M}\mathbf{Q}, \mathbf{Q}^T\,{}^2\mathbf{M}\mathbf{Q}) \;\forall\; \mathbf{Q} \in SO(3)\,. \tag{22}$$

Discarding the cubic invariant I_6 in Φ we arrive at a quadratic form in terms of the invariants and six independent material parameters $\eta_i | i = 1, ..., 6$, respectively

$$\Phi = \eta_1\, I_1 + \eta_2\, I_2 + \eta_3\, I_3 + \eta_4\, I_4^2 + \eta_5\, I_5^2 + \eta_6\, I_4 I_5 - \left(1 + \frac{\hat{\xi}(e^p)}{Y_{11}^0}\right)^2\,. \tag{23}$$

Remark: It can be shown, see CASEY & NAGHDI [9], [10], GREEN & NAGHDI[13] or TSAKMAKIS [39], that under rigid body rotations $\mathbf{Q}$ superposed on the current configuration and – simultanuously – rigid body rotations $\bar{\mathbf{Q}}$ on the intermediate configuration the following transformation rules apply

$$\begin{aligned} \mathbf{F} \;&\rightarrow\; \mathbf{F}^* = \mathbf{Q}\,\mathbf{F} = \mathbf{Q}\,\mathbf{F}^e\,\bar{\mathbf{Q}}^T\,\bar{\mathbf{Q}}\,\mathbf{F}^p = \mathbf{Q}\,\bar{\mathbf{F}}^e\,\bar{\mathbf{F}}^p\;, \\ (\,)\;&\rightarrow\; (\,)^* = \bar{\mathbf{Q}}\;(\,)\;\bar{\mathbf{Q}}^T \quad \text{for} \quad \mathbf{C}^e\,,\,\hat{\mathbf{S}}\,,\,\boldsymbol{\Sigma}\,,\,\mathbf{D}^p\;, \\ \mathbf{L}^p \;&\rightarrow\; \mathbf{L}^{p\,*} = \bar{\mathbf{Q}}\,\mathbf{L}^p\,\bar{\mathbf{Q}}^T + \dot{\bar{\mathbf{Q}}}\,\bar{\mathbf{Q}}^T\;, \end{aligned} \tag{24}$$

where we have restricted ourselves to tensorial quantities of the intermediate configuration playing an eminent role in the present formulation. Invariance of constitutive equations under rigid body rotations superposed on the current configuration is generally required by the principle of material frame indifference, the latter invariance requirement is due to the well known fact, that the multiplicative decomposition is uniquely defined except for a rigid body rotation superposed on the intermediate configuration; the identity $\bar{\mathbf{Q}}^T\,\bar{\mathbf{Q}}$ can always be inserted, in between $\mathbf{F}^e$ and $\mathbf{F}^p$, see $(24)_1$. As a consequence of the constitutive assumption, that only the symmetric part $\hat{\boldsymbol{\sigma}}_s$ enters the yield function, the flow rule reads $\mathbf{D}^p = \lambda\,\partial_{\Sigma_s}\Phi$, which is, see $(24)_2$, invariant with respect to the arbitrary choice of $\bar{\mathbf{Q}}$, whereas this is not true for the plastic velocity gradient $\mathbf{L}^p$ due to the expression $\dot{\bar{\mathbf{Q}}}\,\bar{\mathbf{Q}}^T$ in $(24)_3$.
As a further consequence of the yield function in terms of $\hat{\boldsymbol{\sigma}}_s$ the six independent material parameters $\eta_i | i = 1, ..., 6$ can be experimentally identified by three tension tests and three shear tests, respectively, which are independent of each other.

Assume the tests are performed relative to the fixed orientation of the specimen ${}^1\mathbf{a} = (1,0,0)^T$ and ${}^2\mathbf{a} = (0,1,0)^T$. Let Y^0_{ij} be the yield stress in ij-direction, with respect to ${}^i\mathbf{a}$ and ${}^j\mathbf{a}$. The tests with $\hat{\boldsymbol{\beta}} = \mathbf{0}$ are:

1. uniaxial tension in ${}^1\mathbf{a}$-direction:

$$\boldsymbol{\Sigma}_s = \begin{pmatrix} Y^0_{11} & & \\ & 0 & \\ & & 0 \end{pmatrix} \qquad \left.\begin{array}{ll} I_1 = 2/3(Y^0_{11})^2\,,\, I_4 &= \;\; 2/3Y^0_{11} \\ I_2 = 4/9(Y^0_{11})^2\,,\, I_5 &= -1/3\,Y^0_{11} \\ I_3 = 1/9(Y^0_{11})^2\,,\, I_4\,I_5 &= -2/9\,(Y^0_{11})^2 \end{array}\right\} \tag{25}$$

2. shear test in ${}^1\mathbf{a}$-${}^2\mathbf{a}$ plane:

$$\boldsymbol{\Sigma}_s = \begin{pmatrix} 0 & Y^0_{12} & \\ Y^0_{12} & 0 & \\ & & 0 \end{pmatrix} \qquad \left.\begin{array}{ll} I_1 = 2(Y^0_{12})^2\,,\, I_4 &= 0 \\ I_2 = \;\; (Y^0_{12})^2\,,\, I_5 &= 0 \\ I_3 = \;\; (Y^0_{12})^2\,,\, I_4\,I_5 &= 0 \end{array}\right\} \tag{26}$$

We omit an explicit description of the two uniaxial tension tests in ${}^2\mathbf{a}$- and ${}^3\mathbf{a}$-directions and the two shear tests in ${}^1\mathbf{a}$-${}^3\mathbf{a}$ and ${}^2\mathbf{a}$-${}^3\mathbf{a}$ planes, respectively;

analogously each of them leads to a new set of values for the invariants. Evaluating the flow criterion for all six distinct tests yields the linear equations

$$\begin{bmatrix} \frac{2}{3}(Y_{11}^0)^2 & \frac{4}{9}(Y_{11}^0)^2 & \frac{1}{9}(Y_{11}^0)^2 & \frac{4}{9}(Y_{11}^0)^2 & \frac{1}{9}(Y_{11}^0)^2 & -\frac{2}{9}(Y_{11}^0)^2 \\ \frac{2}{3}(Y_{22}^0)^2 & \frac{1}{9}(Y_{22}^0)^2 & \frac{4}{9}(Y_{22}^0)^2 & \frac{1}{9}(Y_{22}^0)^2 & \frac{4}{9}(Y_{22}^0)^2 & -\frac{2}{9}(Y_{22}^0)^2 \\ \frac{2}{3}(Y_{33}^0)^2 & \frac{1}{9}(Y_{33}^0)^2 & \frac{1}{9}(Y_{33}^0)^2 & \frac{1}{9}(Y_{33}^0)^2 & \frac{1}{9}(Y_{33}^0)^2 & \frac{1}{9}(Y_{33}^0)^2 \\ 2(Y_{12}^0)^2 & (Y_{12}^0)^2 & (Y_{12}^0)^2 & 0 & 0 & 0 \\ 2(Y_{13}^0)^2 & (Y_{13}^0)^2 & 0 & 0 & 0 & 0 \\ 2(Y_{23}^0)^2 & 0 & (Y_{23}^0)^2 & 0 & 0 & 0 \end{bmatrix} \begin{bmatrix} \eta_1 \\ \eta_2 \\ \eta_3 \\ \eta_4 \\ \eta_5 \\ \eta_6 \end{bmatrix} = \begin{bmatrix} 1 \\ 1 \\ 1 \\ 1 \\ 1 \\ 1 \end{bmatrix} \tag{27}$$

with the solution

$$\begin{aligned} \eta_1 &= \frac{1}{2}\left(-\frac{1}{(Y_{12}^0)^2} + \frac{1}{(Y_{13}^0)^2} + \frac{1}{(Y_{23}^0)^2}\right) , \\ \eta_2 &= \frac{1}{(Y_{12}^0)^2} - \frac{1}{(Y_{23}^0)^2} , \\ \eta_3 &= \frac{1}{(Y_{12}^0)^2} - \frac{1}{(Y_{13}^0)^2} , \\ \eta_4 &= \frac{2}{(Y_{11}^0)^2} - \frac{1}{(Y_{22}^0)^2} + \frac{2}{(Y_{33}^0)^2} - \frac{1}{(Y_{13}^0)^2} , \\ \eta_5 &= -\frac{1}{(Y_{11}^0)^2} + \frac{2}{(Y_{22}^0)^2} + \frac{2}{(Y_{33}^0)^2} - \frac{1}{(Y_{23}^0)^2} , \\ \eta_6 &= -\frac{1}{(Y_{11}^0)^2} - \frac{1}{(Y_{22}^0)^2} + \frac{5}{(Y_{33}^0)^2} + \frac{1}{(Y_{12}^0)^2} - \frac{1}{(Y_{13}^0)^2} - \frac{1}{(Y_{23}^0)^2} . \end{aligned} \tag{28}$$

Now we consider pure isotropy as a special case of orthotropy. For isotropic elasticity $\boldsymbol{\Sigma} = \boldsymbol{\Sigma}^T$ holds and therefore $\mathbf{L}^p = \mathbf{D}^p$. In this case our constitutive assumption for Φ being a function merely of the symmetric part of $\boldsymbol{\Sigma}$ is fulfilled by the elasticity law itself. If we set for the yield normal stresses $Y_{ii}^0 = Y^0$ for $i = 1, 2, 3$ and for the yield shear stresses $Y_{ij}^0 = Y^0/\sqrt{3}$ for $i \neq j$ with $i, j = 1, 2, 3$ we arrive at the isotropic von Mises yield criterion

$$\hat{\Phi}(\mathrm{dev}\hat{\boldsymbol{\sigma}}, \xi) = \frac{3}{2}\left(\frac{||\mathrm{dev}\hat{\boldsymbol{\sigma}}||}{Y^0}\right)^2 - \left(1 + \frac{\hat{\xi}(e^p)}{Y^0}\right)^2 \leq 0 . \tag{29}$$

In the computational benchmark problems in Sect. 6 we apply a nonlinear isotropic hardening function well suited for a fitting of experimental data

$$\hat{\xi}(e^p) = he^p + (Y^\infty - Y^0)(1 - \exp(-\delta e^p)) , \tag{30}$$

where the expression in terms of Y^∞, Y^0 and δ in (30) is of saturation type.

The constitutive equations are now summarized as follows.

$$
\begin{array}{lll}
\text{elastic strains} & \mathbf{C}^e &= \mathbf{F}^{p\,T-1}\,\mathbf{C}\,\mathbf{F}^{p\,-1} \\
\text{free energy} & \psi &= \hat{\psi}^e(J_1,...,J_6) + \hat{\psi}^{p,iso}(e^p) + \hat{\psi}^{p,kin}(\boldsymbol{\alpha}) \\
\text{stresses} & \hat{\mathbf{S}} &= 2\,\partial_{C^e}\psi^e \quad , \quad \boldsymbol{\Sigma} = \mathbf{C}^e\,\hat{\mathbf{S}} \\
\text{back stresses} & \hat{\boldsymbol{\beta}} &= \partial_\alpha \psi^{p,kin} \\
\text{isotropic hardening} & \xi &= \partial_{e^p}\psi^{p,iso} \\
\text{relative stresses} & \hat{\boldsymbol{\sigma}}_s &= \boldsymbol{\Sigma}_s - \hat{\boldsymbol{\beta}}_s \\
\text{yield function} & \Phi &= \hat{\Phi}(I_1,...,I_5,\xi) \\
\text{associative flow rule} & \mathbf{D}^p &= \lambda\,\partial_{\boldsymbol{\Sigma}_s}\Phi \\
\text{evolution of } \boldsymbol{\alpha} & \dot{\boldsymbol{\alpha}} &= -\lambda\,\partial_{\hat{\beta}_s}\Phi \\
\text{evolution of } e^p & \dot{e}^p &= \sqrt{\tfrac{2}{3}}||\mathbf{D}^p|| \\
\text{optimization conditions} & \lambda \geq 0,\ \Phi \leq 0, & \lambda\Phi = 0
\end{array}
\tag{31}
$$

3 Integration Algorithm for the Constitutive Equations

To solve the set of constitutive equations at a local level, a so-called operator split along with a general return mapping is applied; for time integration a backward Euler scheme with an exponential map is used. For the solution of the nonlinear finite-element equations on a global level a Newton iteration scheme is used, which requires the consistent tangent matrix. For this reason a simple numerical differentiation technique is applied.

3.1 General Return Algorithm

Based on the definition $(5)_2$ of $\mathbf{L}^p$, and taking $\mathbf{L}^p = \mathbf{D}^p$ into account, we write the flow rule $(31)_8$ for $\mathbf{D}^p$ as

$$
\dot{\mathbf{F}}^p = \mathbf{D}^p\mathbf{F}^p = \lambda \mathbf{N}\,\mathbf{F}^p \quad \text{with} \quad \mathbf{N} := \frac{\partial \Phi}{\partial \boldsymbol{\Sigma}_s}\,. \tag{32}
$$

Within a typical time step $[t_n\,,\,t_{n+1}]$ with time increment $\Delta t := t_{n+1} - t_n$ we integrate (32) by the implicit backward Euler algorithm along with an exponential shift

$$
\mathbf{F}^p_{n+1} = \exp[\gamma\,\partial_{\Sigma_s}\Phi_{n+1}]\;\mathbf{F}^p_n\,, \tag{33}
$$

where $\gamma := \Delta t\,\lambda_{n+1}$ denotes the consistency parameter. For $\mathbf{N}$ we use the corresponding tensor of the trial step defined below. For deviatoric $\mathbf{N}$, i.e. $\mathrm{tr}[\mathbf{N}] = 0$, and applying the identity $\det(\exp[\mathbf{N}]) = \exp[\mathrm{tr}(\mathbf{N})]$, it is obvious that the exponential map (33) preserves plastic incompressibility in the current time step, given that $\det \mathbf{F}^p_n = 1$ holds for the previous step. The

rate equations for $\boldsymbol{\alpha}$ and e^p are integrated using a standard backward Euler algorithm. Thus, the procedure for time integration is first order accurate and unconditionally stable. Considering the multiplicative decomposition we obtain for the update of the elastic Cauchy–Green tensor

$$\begin{aligned}\mathbf{C}^e_{n+1} &= \mathbf{F}^{p\,T-1}_{n+1}\,\mathbf{C}_{n+1}\,\mathbf{F}^{p\,-1}_{n+1} \\ &= \exp^T[-\gamma_{n+1}\,\mathbf{N}^{trial}_{n+1}]\,\mathbf{C}^{e\,trial}_{n+1}\,\exp[-\gamma_{n+1}\,\mathbf{N}^{trial}_{n+1}]\,,\end{aligned} \tag{34}$$

where we have introduced by definition $\mathbf{C}^{e\,trial}_{n+1} := \mathbf{F}^{p\,T-1}_{n}\,\mathbf{C}_{n+1}\,\mathbf{F}^{p\,-1}_{n}$ as elastic trial strains. It is well known that for the case of isotropic elasticity $\mathbf{N}_{n+1}$ and $\mathbf{C}^e_{n+1}$ commute, i.e. they have the same principal directions, which allows for a stress update formula that is identical to the classical return mapping algorithm of the geometrically linear theory, see Miehe & Stein [22] and Simo [32].
With the trial values for the Mandel stresses

$$\boldsymbol{\Sigma}^{trial}_{n+1} \;=\; 2\;\mathbf{C}^{e\,trial}_{n+1}\,\partial_{\mathbf{C}^{e\,trial}_{n+1}}\psi^e\,, \tag{35}$$

and for the internal variables, i.e. the back stresses $\hat{\boldsymbol{\beta}}^{trial}_{n+1} = \partial_{\boldsymbol{\alpha}_n}\;\psi^{p,kin}$ and the equivalent plastic strain $e^{p\,trial}_{n+1} = \partial_{\xi_n}\;\psi^{p,iso}$ we obtain a trial value for the yield criterion in terms of the deviatoric part of the symmetric relative stresses $\mathrm{dev}\hat{\boldsymbol{\sigma}}_s$ as follows:

$$\Phi^{trial}_{n+1} = \hat{\Phi}(\mathrm{dev}\hat{\boldsymbol{\sigma}}^{trial}_{s}\;,\;\overset{i}{\mathbf{M}}, e^p_n)^{trial}_{n+1}\,. \tag{36}$$

The time discrete consistency condition reads in the case of plastic loading $\Phi_{n+1} \;=\; 0$, which can be solved for γ_{n+1} by applying a Newton solution scheme. At the end of each local iteration the intermediate configuration, described by $\mathbf{F}^p_{n+1}$, and the internal variables $\boldsymbol{\alpha}_{n+1}$ and e^p_{n+1} have to be updated. A summary of the general return mapping algorithm is given in (40) below.

3.2 Algorithmic Elastoplastic Moduli

As we use an Lagrangian formulation of the weak form, which is outlined in Sect. 4, the Second Piola–Kirchhoff stress tensor must be determined by pull back transformation $\mathbf{S} = \mathbf{F}^{p\,-1}\hat{\mathbf{S}}\mathbf{F}^{p\,T-1}$. The nonlinear finite element equations are solved by using a Newton iteration scheme. For this purpose the so-called consistent tangent matrix

$$\mathbb{C}_{ep} = 2\partial\mathbf{S}/\partial\mathbf{C} = \mathbb{C}^{ABCD}\mathbf{e}_A\otimes\mathbf{e}_B\otimes\mathbf{e}_C\otimes\mathbf{e}_D \tag{37}$$

is approximated by numerical differentiation. To this end a simple perturbation technique is applied using the forward difference formula

$$\mathbb{C}^{ABCD} \approx \frac{2}{\epsilon}\left[S^{AB}(\mathbf{C}^{\epsilon}_{(CD)}) - S^{AB}\right]\,. \tag{38}$$

The perturbed Cauchy–Green tensor is computed as

$$\mathbf{C}^{\epsilon}_{(CD)} := \mathbf{C} + \Delta\mathbf{C}^{\epsilon}_{(CD)} \;\text{ with }\; \Delta\mathbf{C}^{\epsilon}_{(CD)} = \frac{\epsilon}{2}\left(\mathbf{e}_C \otimes \mathbf{e}_D + \mathbf{e}_D \otimes \mathbf{e}_C\right) , \quad (39)$$

where $\mathbf{e}_I$, $I = A, B, C, D$ denotes a fixed Cartesian basis. Computations have shown, that $\epsilon = 10^{-7}$ provides a good choice for the perturbation parameter. As the numerical differentiation requires six additional stress computations, it costs more CPU time than the analytical computation of the moduli. Nevertheless, the numerical determination of consistent algorithmic moduli is advantageous for its simplicity, robustness and for being independent of the material model. It serves as an interface for implementing complicated constitutive models without tedious analytical derivations of tangent operators.

---

1. `Trial step - elastic predictor`

$$\mathbf{C}^{e\,trial}_{n+1} = \mathbf{F}^{p\,T-1}_{n}\,\mathbf{C}_{n+1}\,\mathbf{F}^{p\,-1}_{n}$$

$$\boldsymbol{\Sigma}^{trial}_{n+1} = 2\,\mathbf{C}^{e\,trial}_{n+1}\frac{\partial\psi^{e}}{\partial\mathbf{C}^{e\,trial}_{n+1}} \;,\; \hat{\boldsymbol{\beta}}^{trial}_{n+1} = \frac{\partial\psi^{p,kin}}{\partial\boldsymbol{\alpha}_n}$$

$$\hat{\boldsymbol{\sigma}}^{trial}_{n+1} := \boldsymbol{\Sigma}^{trial}_{n+1} - \hat{\boldsymbol{\beta}}^{trial}_{n+1} \;,\; \mathbf{N}^{trial}_{n+1} = \frac{\partial\Phi}{\partial\boldsymbol{\Sigma}^{trial}_{s\,n+1}}$$

2. `Check yield condition`

`if` $\hat{\Phi}(\mathrm{dev}\hat{\boldsymbol{\sigma}}^{trial}_{s\,n+1}, \overset{i}{\mathbf{M}}, e^{p}_{n}) > 0$ `go to 3. else exit`

3. `Return mapping - corrector step`

`set` $\gamma^{(0)}_{n+1} = 0 \;,\; e^{p(0)}_{n+1} = e^{p}_{n} \;,\; \boldsymbol{\alpha}^{(0)}_{n+1} = \boldsymbol{\alpha}_n$

a) $$\mathbf{C}^{e(l)}_{n+1} = \exp^{T}[-\gamma^{(l)}_{n+1}\,\mathbf{N}^{trial}_{n+1}]\,\mathbf{C}^{e\,trial}_{n+1}\,\exp[-\gamma^{(l)}_{n+1}\,\mathbf{N}^{trial}_{n+1}] \quad (40)$$

$$e^{p(l)}_{n+1} = e^{p}_{n} + \gamma^{(l)}_{n+1}\sqrt{\frac{2}{3}}\|\mathbf{N}^{trial}_{n+1}\| \;,\; \boldsymbol{\alpha}^{(l)}_{n+1} = \boldsymbol{\alpha}_n + \gamma^{(l)}_{n+1}\,\mathbf{N}^{trial}_{n+1}$$

b) $$\boldsymbol{\Sigma}^{(l)}_{n+1} = 2\,\mathbf{C}^{e(l)}_{n+1}\frac{\partial\psi^{e}}{\partial\mathbf{C}^{e(l)}_{n+1}} \;,\; \hat{\boldsymbol{\beta}}^{(l)}_{n+1} = \frac{\partial\psi^{p,kin}}{\partial\boldsymbol{\alpha}^{(l)}_{n+1}} \;,\; \xi^{(l)}_{n+1} = \frac{\partial\psi^{p,iso}}{\partial e^{p(l)}{}_{n+1}}$$

c) $$\Phi^{(l)}_{n+1} = \Phi(\gamma^{(l)}_{n+1}) \;,\; \Phi'^{(l)}_{n+1} \approx [\Phi(\gamma^{(l)}_{n+1} + \epsilon) - \Phi(\gamma^{(l)}_{n+1})]/\epsilon$$

`if` $|\Phi^{(l)}_{n+1}| \le$ `tol` `go to 4.`

d) $$\gamma^{(l+1)}_{n+1} = \gamma^{(l)}_{n+1} - \Phi^{(l)}_{n+1}/\Phi'^{(l)}_{n+1}$$ `go to a)`

4. `Update intermediate configuration and internal variables`

$$\mathbf{F}^{p}_{n+1} = \exp[\gamma^{(l)}_{n+1}\mathbf{N}^{trial}_{n+1}]\;\mathbf{F}^{p}_{n} \;,\; e^{p}_{n+1} = e^{p(l)}_{n+1} \;,\; \boldsymbol{\alpha}_{n+1} = \boldsymbol{\alpha}^{(l)}_{n+1}$$

3.3 Efficient Calculation of the Exponential Map

For an effective computation of the exponential function of a second order tensor $\boldsymbol{\beta}$ which is not necessarily symmetric we use an recursive algorithm, see MIEHE [23], SANSOUR & KOLLMANN[30]. Firstly, we recall that $\exp[\boldsymbol{\beta}]$ is defined by the power-series

$$\exp[\boldsymbol{\beta}] = \mathbf{1} + \boldsymbol{\beta} + \frac{1}{2!}\boldsymbol{\beta}^2 + \frac{1}{3!}\boldsymbol{\beta}^3 + \ldots + \frac{1}{n!}\boldsymbol{\beta}^n + \ldots \ . \tag{41}$$

Let I_1,I_2,I_3 denote the principal invariants of $\boldsymbol{\beta}$

$$I_1 = \mathrm{tr}[\boldsymbol{\beta}] \ , \ I_2 = \tfrac{1}{2}(I_1^2 - \mathrm{tr}[\boldsymbol{\beta}^2]) \ , \ I_3 = \det[\boldsymbol{\beta}] \ . \tag{42}$$

The Cayley–Hamilton theorem for $\boldsymbol{\beta}$ reads

$$\boldsymbol{\beta}^3 = I_3\mathbf{1} - I_2\boldsymbol{\beta} + I_1\boldsymbol{\beta}^2 \ . \tag{43}$$

Since $\exp[\boldsymbol{\beta}]$ is an isotropic tensor-function of $\boldsymbol{\beta}$, the representation theorem of Rivlin–Ericksen gives

$$\exp[\boldsymbol{\beta}] = \alpha_0(I_1, I_2, I_3)\mathbf{1} + \alpha_1(I_1, I_2, I_3)\boldsymbol{\beta} + \alpha_2(I_1, I_2, I_3)\boldsymbol{\beta}^2 \ . \tag{44}$$

The goal, to calculate $\exp[\boldsymbol{\beta}]$ in an efficient way is achieved by a successive application of the Cayley–Hamilton theorem (43), which allows for a representation of the third and higher powers of $\boldsymbol{\beta}$ in (41) in terms of $\mathbf{1}, \boldsymbol{\beta}, \boldsymbol{\beta}^2$. Thus we achieve the power-series of $\exp[\boldsymbol{\beta}]$ (41) in the representation of (44),

$$\boldsymbol{\beta}^n = \gamma_0^{(n)}\mathbf{1} + \gamma_1^{(n)}\boldsymbol{\beta} + \gamma_2^{(n)}\boldsymbol{\beta}^2 \ , \tag{45}$$

with $\gamma_0^{(n)}$,$\gamma_1^{(n)}$,$\gamma_2^{(n)}$ as functions of the invariants of $\boldsymbol{\beta}$. It can be easily shown by induction, that for arbitrary n the coefficients $\gamma_0^{(n)}$,$\gamma_1^{(n)}$,$\gamma_2^{(n)}$ can be calculated as functions of $\gamma_0^{(n-1)}$,$\gamma_1^{(n-1)}$,$\gamma_2^{(n-1)}$ according to the following recursion formula

$$\left.\begin{array}{rl} \gamma_0^{(n)} = & I_3\gamma_0^{(n-1)} \\ \gamma_1^{(n)} = \gamma_0^{(n-1)} & - I_2\gamma_2^{(n-1)} \\ \gamma_2^{(n)} = \gamma_1^{(n-1)} & + I_1\gamma_2^{(n-1)} \end{array}\right\} \ . \tag{46}$$

Comparison of the coefficients in (46) and (44) yields for α_0, α_1, α_2

$$\left.\begin{array}{l} \alpha_0 = 1 + \dfrac{1}{3!}I_3 + \displaystyle\sum_{n=4}^{N}\frac{1}{n!}\gamma_0^{(n)} \quad , \quad \alpha_1 = 1 - \dfrac{1}{3!}I_2 + \displaystyle\sum_{n=4}^{N}\frac{1}{n!}\gamma_1^{(n)} \\ \alpha_2 = \dfrac{1}{2} + \dfrac{1}{3!}I_1 + \displaystyle\sum_{n=4}^{N}\frac{1}{n!}\gamma_2^{(n)} \end{array}\right\} \ , \tag{47}$$

or with $\gamma_0^{(1)} = 1\,,\ \gamma_1^{(1)} = 1\,,\ \gamma_2^{(1)} = 0\,,\ \gamma_0^{(2)} = 0\,,\ \gamma_1^{(2)} = 0\,,\ \gamma_2^{(2)} = 1\,,\ \gamma_0^{(3)} = I_3\,,\ \gamma_1^{(3)} = -I_2\,,\ \gamma_2^{(3)} = I_1$, we obtain the parameters $\alpha_0, \alpha_1, \alpha_2$ in (44) as

$$\alpha_0 = \sum_{n=1}^{N} \frac{1}{n!}\gamma_0^{(n)}\ ,\ \alpha_1 = \sum_{n=1}^{N} \frac{1}{n!}\gamma_1^{(n)}\ ,\ \alpha_2 = \sum_{n=1}^{N} \frac{1}{n!}\gamma_2^{(n)}\ . \tag{48}$$

The number N depends on the desired accuracy up to which the exponential series is evaluated. With a chosen tolerance `tol` we define the stop criterion as

$$\frac{\gamma_i^{(n)}}{n!} < \texttt{tol}\ ,\ \ i = 1,2,3\,. \tag{49}$$

An alternative method to fulfill the plastic incompressibility condition, which is based on a simple post-processing step, was proposed by the authors in [12], [14] within a formulation of isotropic elastoplasticity using Almansi strain tensors.

4 Variational Formulation

Let $\mathcal{B}$ be the reference body of interest which is bounded by the surface $\partial\mathcal{B}$. The surface is partitioned into two disjoint parts $\partial\mathcal{B} = \partial\mathcal{B}_u \bigcup \partial\mathcal{B}_t$ with $\partial\mathcal{B}_u \bigcap \partial\mathcal{B}_t = \emptyset$. The equation of balance of linear momentum for the static case is governed by the First Piola–Kirchhoff stresses $\mathbf{P} = \mathbf{FS}$ and the body force $\hat{\mathbf{b}}$ in the reference configuration

$$\mathrm{Div}[\mathbf{FS}] + \hat{\mathbf{b}} = \mathbf{0}\,. \tag{50}$$

The Dirichlet and Neumann boundary conditions are given by $\mathbf{u} = \bar{\mathbf{u}}$ on $\partial\mathcal{B}_u$ and $\mathbf{t} = \hat{\mathbf{t}} = \mathbf{PN}$ on $\partial\mathcal{B}_t$, respectively. Here $\hat{\mathbf{t}}$ denotes surface loads, $\mathbf{N}$ represents the exterior unit normal to the boundary surface $\partial\mathcal{B}_t$. With standard arguments of variational calculus we arrive at the variational problem

$$G(\mathbf{u}, \delta\mathbf{u}) = \int_{\mathcal{B}} \mathbf{S} : \delta\mathbf{E}\ dV + G^{ext}\ , \quad \text{with} \tag{51}$$

$$G^{ext}(\delta\mathbf{u}) := -\int_{\mathcal{B}} \hat{\mathbf{b}}\,\delta\mathbf{u}\ dV - \int_{\partial\mathcal{B}_t} \hat{\mathbf{t}}\,\delta\mathbf{u}\ dA\ , \tag{52}$$

where $\delta\mathbf{E} := \frac{1}{2}(\delta\mathbf{F}^T\mathbf{F} + \mathbf{F}^T\delta\mathbf{F})$ characterizes the virtual Green–Lagrangian strain tensor in terms of the virtual deformation gradient $\delta\mathbf{F} := \mathrm{Grad}\delta\mathbf{u}$. The equation of principle of virtual work (51) for a static equilibrium state of the considered body requires $G = 0$. For the solution of this nonlinear equation a standard Newton iteration scheme is applied, which requires the consistent linearization of (51) in order to guarantee quadratic convergence rate near

the solution. Since the stress tensor $\mathbf{S}$ is symmetric, the linear increment of G denoted by ΔG is given by

$$\Delta G(\mathbf{u}, \delta\mathbf{u}, \Delta\mathbf{u}) := \int_{\mathcal{B}} (\delta\mathbf{E} : \Delta\mathbf{S} + \Delta\delta\mathbf{E} : \mathbf{S})\, dV \,, \tag{53}$$

where $\Delta\delta\mathbf{E} := \frac{1}{2}(\Delta\mathbf{F}^T\delta\mathbf{F} + \delta\mathbf{F}^T\Delta\mathbf{F})$ denotes the linearized virtual Green–Lagrange strain tensor as a function of the incremental deformation gradient $\Delta\mathbf{F} := \mathrm{Grad}\Delta\mathbf{u}$. The incremental Second Piola–Kirchhoff stress tensor $\Delta\mathbf{S}$ can be derived as $\Delta\mathbf{S} = \mathbb{C}_{ep}\Delta\mathbf{E}$ with $\Delta\mathbf{E} := \frac{1}{2}(\Delta\mathbf{F}^T\mathbf{F} + \mathbf{F}^T\Delta\mathbf{F})$ and the consistent tangent matrix $\mathbb{C}_{ep}$.

5 Finite Element Discretization

For numerical analyses of thin structures with finite elements it is crucial to avoid *locking*, i.e. artificial stiffening effects. Such effects occur when simple low-order, displacement type elements are used. For an overview with detailed explanations of the sources of different *locking* effects we refer to Klinkel [20]. In this section we describe different effective remedies against this undesired stiffening.
We firstly introduce the formulation of a standard displacement type element. Hence certain modifications are necessary to reduce the locking effects. To avoid *shear locking* the transverse shear strains are approximated by using the interpolation functions of Bathe & Dvorkin [1]. Artificial thickness strains can be avoided by using the interpolation functions of Betsch & Stein [4].

5.1 Displacement Type Formulation

According to the isoparametric concept we use the standard tri-linear shape functions for an eight-node ($nel = 8$) solid element to interpolate the geometry of the initial and the current configurations

$$\mathbf{X}^h = \sum_{I=1}^{nel} N_I(\xi^1, \xi^2, \xi^3)\mathbf{X}_I \quad , \quad \mathbf{x}^h = \sum_{I=1}^{nel} N_I(\xi^1, \xi^2, \xi^3)\mathbf{x}_I \quad \text{with} \tag{54}$$

$$N_I(\xi^1, \xi^2, \xi^3) = \frac{1}{8}(1 + \xi_I^1\xi^1)(1 + \xi_I^2\xi^2)(1 + \xi_I^3\xi^3)\,. \tag{55}$$

The index h denotes the finite element discretization. The convective base vectors of the initial and the current configurations are

$$\mathbf{G}_i^h = \sum_{I=1}^{nel} N_{I,i}\ \mathbf{X}_I \quad , \quad \mathbf{g}_i^h = \sum_{I=1}^{nel} N_{I,i}\ \mathbf{x}_I \,, \tag{56}$$

and the approximation of the virtual strains is given by

$$\delta \mathbf{E}^h = \sum_{I=1}^{nel} \mathbf{B}_I \delta \mathbf{v}_I \quad , \quad \mathbf{B}_I = [\mathbf{B}_I^m, \mathbf{B}_I^s]^T \quad . \tag{57}$$

The components of the virtual nodal displacement vector $\delta \mathbf{v}_I$ are given with respect to the fixed Cartesian basis system. The matrices $\mathbf{B}_I^m$ and $\mathbf{B}_I^s$ are specified below. The expression $\mathbf{S} : \Delta\delta\mathbf{E}^h$ leads to the geometrical matrix $\mathbf{G}_{IJ}$ where the linearized virtual strains $\Delta\delta\mathbf{E}$ were explicitly given above,

$$\mathbf{S} : \Delta\delta\mathbf{E}^h = \sum_{I=1}^{nel} \sum_{J=1}^{nel} \delta \mathbf{v}_I^T \; \mathbf{G}_{IJ} \; \Delta \mathbf{v}_J \quad , \quad \mathbf{G}_{IJ} = \mathrm{diag}\,[S_{IJ},\, S_{IJ},\, S_{IJ}] \; . \tag{58}$$

The expression $S_{IJ} = S_{IJ}^m + S_{IJ}^s$ results from two parts specified below.

5.2 Shear Stiffness Part

According to Fig. 5.1, four collocation points $M = A, B, C, D$ with given coordinates ξ^i are defined.

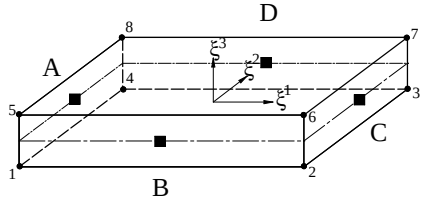

$$A = \begin{pmatrix} -1, & 0, & 0 \end{pmatrix}$$
$$B = \begin{pmatrix} 0, & -1, & 0 \end{pmatrix}$$
$$C = \begin{pmatrix} 1, & 0, & 0 \end{pmatrix}$$
$$D = \begin{pmatrix} 0, & 1, & 0 \end{pmatrix}$$

Fig. 5.1 Collocation points of the shear strain interpolation

At these points, the shear strains E_{13}^M, E_{23}^M of the Green–Lagrangian strain tensor are evaluated. To overcome *shear locking*, the transverse shear strains E_{13} and E_{23} are obtained via the interpolation in the ξ^1-ξ^2-plane,

$$\begin{bmatrix} 2E_{13}^h \\ 2E_{23}^h \end{bmatrix} = \begin{bmatrix} (1-\xi^2)E_{13}^B + (1+\xi^2)E_{13}^D \\ (1-\xi^1)E_{23}^A + (1+\xi^1)E_{23}^C \end{bmatrix} \quad . \tag{59}$$

According to (59) the transverse shear strains are assumed to be constant in thickness direction within the considered element. Numerical tests have shown that this approximation is sufficient for thin structures. The alternative with two planes and eight collocation points within the element does not lead to significant differences. Hence, the variation of the transverse shear strains can be expressed as

$$\begin{bmatrix} 2\delta E_{13}^h \\ 2\delta E_{23}^h \end{bmatrix} = \sum_{I=1}^{nel} \mathbf{B}_I^s \, \delta \mathbf{v}_I \quad , \quad \text{with} \tag{60}$$

$$\mathbf{B}_I^s = \frac{1}{2}\begin{bmatrix} (1-\xi^2)(\mathbf{g}_3^{B^T} N_{I,1}^B + \mathbf{g}_1^{B^T} N_{I,3}^B) + (1+\xi^2)(\mathbf{g}_3^{D^T} N_{I,1}^D + \mathbf{g}_1^{D^T} N_{I,3}^D) \\ (1-\xi^1)(\mathbf{g}_3^{A^T} N_{I,2}^A + \mathbf{g}_2^{A^T} N_{I,3}^A) + (1+\xi^1)(\mathbf{g}_3^{C^T} N_{I,2}^C + \mathbf{g}_2^{C^T} N_{I,3}^C) \end{bmatrix}. \tag{61}$$

The shape function N_I^M and the current base vectors $\mathbf{g}_i^M$ are obtained by exploitation of the corresponding equation at the collocation points M. The above defined quantity S_{IJ}^s reads

$$\begin{aligned} &S_{IJ}^s = \\ &\tfrac{1}{2}[(1-\xi^2)(N_{I,1}^B\ N_{J,3}^B + N_{I,3}^B\ N_{J,1}^B) + (1+\xi^2)(N_{I,1}^D\ N_{J,3}^D + N_{I,3}^D\ N_{J,1}^D)]\ S^{13} \\ &+\tfrac{1}{2}[(1-\xi^1)(N_{I,2}^A\ N_{J,3}^A + N_{I,3}^A\ N_{J,2}^A) + (1+\xi^1)(N_{I,2}^C\ N_{J,3}^C + N_{I,3}^C\ N_{J,2}^C)]\ S^{23}. \end{aligned} \tag{62}$$

5.3 Approximation of the Thickness Strain

For thin shell structures with bending dominated loading a *locking* effect due to artificial thickness strains has been observed by Ramm et al. in [29] when using a direct interpolation of the director vector. To overcome this type of *locking* an *assumed natural strain* (ANS)-interpolation of the thickness strain E_{33} using bi-linear shape functions for four-node shell elements was proposed by Betsch & Stein in [4] and by Bischoff & Ramm in [6]. Here, we adapt this procedure to the eight-node brick element. According to Fig. 5.2 four collocation points $L = A_1,\ A_2,\ A_3,\ A_4$ are defined in the reference surface with $\xi^3 = 0$.

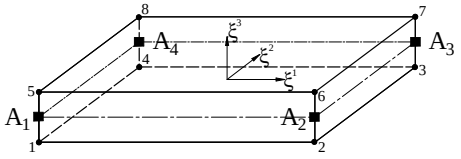

$$\begin{aligned} A_1 &= \big(-1,\ -1,\quad 0\big) \\ A_2 &= \big(\ \ 1,\ -1,\quad 0\big) \\ A_3 &= \big(\ \ 1,\quad 1,\quad 0\big) \\ A_4 &= \big(-1,\quad 1,\quad 0\big) \end{aligned}$$

Fig. 5.2 Collocation points for the thickness strain interpolation

The approximation of E_{33} reads

$$E_{33}^h = \sum_{L=1}^{4} \frac{1}{4}(1+\xi_L^1\xi^1)(1+\xi_L^2\xi^2)\ E_{33}^L \quad , \quad L = A_1,\ A_2,\ A_3,\ A_4\ , \tag{63}$$

where E_{33}^L denotes the thickness strains at the above defined points L. Thus with (63) it is assumed, that within the considered element E_{33} is constant in the ξ^3-direction. This assumption holds for thin structures.
The variation of the thickness strains and the membrane strains are obtained

from

$$\begin{pmatrix} \delta E^h_{11} \\ \delta E^h_{22} \\ \delta E^h_{33} \\ 2\delta E^h_{12} \end{pmatrix} = \sum_{I=1}^{nel} \underbrace{\begin{pmatrix} \mathbf{g}_1^T N_{I,1} \\ \mathbf{g}_2^T N_{I,2} \\ \sum\limits_{L=1}^{4} \frac{1}{4}(1+\xi_L^1\xi^1)(1+\xi_L^2\xi^2)\ (\mathbf{g}_3^L)^T N^L_{I,3} \\ \mathbf{g}_2^T N_{I,1} + \mathbf{g}_1^T N_{I,2} \end{pmatrix}}_{\mathbf{B}^m_I} \delta\mathbf{v}_I \,. \tag{64}$$

Furthermore, the above defined quantity S^m_{IJ} yields

$$\begin{aligned} S^m_{IJ} = \quad & S^{11}\ N_{I,1}N_{I,1} + S^{22}\ N_{I,2}N_{I,2} + S^{12}\ (N_{I,1}N_{I,2} + N_{I,2}N_{I,1}) \\ & + S^{33}\ \sum_{L=1}^{4} \frac{1}{4}(1+\xi_L^1\xi^1)(1+\xi_L^2\xi^2)\ N^L_{I,3}\ N^L_{J,3} \,. \end{aligned} \tag{65}$$

Next, the following stiffness matrices, associated with the element nodes I, J, are introduced

$$\mathbf{K}_{eIJ} = \int\limits_{\mathcal{B}_0^e} (\mathbf{B}_I^T \mathbb{C} \mathbf{B}_J + \mathbf{G}_{IJ})\ \mathrm{d}V \quad , \tag{66}$$

and the vectors

$$\mathbf{f}^{int}_{eI} = \int\limits_{\mathcal{B}_e^0} \mathbf{B}_I^T\ \mathbf{S}\ \mathrm{d}V \quad , \quad \mathbf{f}^{ext}_{eI} = \int\limits_{\mathcal{B}_e^0} N_I\ \rho_0\ \hat{\mathbf{b}}\ \mathrm{d}V + \int\limits_{\partial\mathcal{B}_e^0} N_I \hat{\mathbf{t}}\ \mathrm{d}A \tag{67}$$

are defined. Here, $\mathbf{S}$ denotes the vector of the Second Piola–Kirchhoff stresses obtained by the pull back transformation $\mathbf{S} = \mathbf{F}^{p\,-1}\hat{\mathbf{S}}\mathbf{F}^{p\,T-1}$. Hence, the discretized linearized weak form yields the following system of equations on element level

$$\left[\,\mathbf{K}_e\,\right]\left[\,\Delta\mathbf{v}^e\,\right] \;=\; \left[\,\mathbf{f}^{ext}_e \;-\; \mathbf{f}^{int}_e\,\right]. \tag{68}$$

Here, $\mathbf{K}_e$, $\mathbf{f}^{int}_e$ and $\mathbf{f}^{ext}_e$ contain the submatrices $\mathbf{K}_{eIJ}$, $\mathbf{f}^{int}_{eI}$ and $\mathbf{f}^{ext}_{eI}$ according to the order of the nodes I and J. Furthermore, $\Delta\mathbf{v}^e$ denotes the vector of the incremental element displacements. The spatial discretization of the considered body leads after assembly $\mathcal{B} \approx \bigcup_{e=1}^{n_{ele}} \mathcal{B}^e$ with n_{ele} finite elements $\mathcal{B}^e$ to a set of algebraic equations which can be solved for the unknown nodal displacements.

6 Numerical Examples

The algorithmic formulation of the orthotropic constitutive model derived and analyzed in the previous sections is implemented in an extended version of FEAP, a general nonlinear finite element code documented in [38]. Four sets of simulations are conducted to test the behavior of the proposed orthotropic model as well as the robustness of the numerical methods. The computational simulations are checked to capture qualitatively the *earing* phenomenon owing to the anisotropic nature of rolled sheet metal. Furthermore, we compare our results quantitatively with numerical simulations of other references and – as far as they are available – with experimental data, the latter for isotropy as a special case of orthotropy. All simulations were run with the 8-node brick type shell element using the ANS -method and a 5-parameter EAS concept, respectively.

6.1 Necking of a Circular Bar

The necking of a circular bar is an example widely investigated in the literature, see e.g. Simo & Armero [33] or Klinkel [20]. The geometrical data are $R = 6.413\,\text{mm}$, $R_b = 0.982R$ and $L = 26.667\,\text{mm}$. To initialize the necking process we use the reduced radius R_b at $z = 26.667\,\text{mm}$ as a geometrical imperfection. The material data for isotropic elasticity and the isotropic von Mises yield condition (29) with nonlinear isotropic hardening (30) are given as follows.

Elasticity constants:
$E = 206.9\,\text{GPa}\ ,\ \nu = 0.29$

Yield parameter:
$Y^0 = 0.45\,\text{GPa}\ ,\ Y^\infty = 0.715\,\text{GPa}$
$h = 0.12924\,\text{GPa}\ ,\ \delta = 16.93$

Hardening function:
$\hat{\xi}(e^p) = he^p + (Y^\infty - Y^0)(1 - \exp(-\delta e^p))$

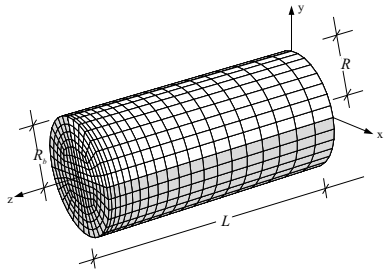

Fig. 6.1. Necking of a circular bar. Elastoplastic material data, geometry and finite element mesh

The finite element discretization of half the bar is depicted in Fig. 6.1. At $z = L$ we impose the symmetry boundary conditions $w = 0\,\text{mm}$, whereas in a displacement controlled computation the axial elongation $w(z = 0\,\text{mm})$ is prescribed. Furthermore, we consider symmetry conditions in the cross-section of the plane. Thus, one eighth of the entire bar of total length $2L$ is discretized with 960 elements, where the thickness direction of the shell elements corresponds to the global z-axis. Figure 6.2 displays the deformed

structure at $w = 7\,\mathrm{mm}$ and the equivalent plastic strain, which concentrates in the necking zone. The results are in very good agreement with the computational reference solutions of Simo & Armero [33] and that of Klinkel [20], see Fig. 6.3. Before the onset of necking the result of our finite element analysis is in accurate accordance with the experimental results reported in Norris et al. [26]; it captures pretty well the load bearing capacity of the bar of 79.2 kN, whereas for elongations $w > 4\,\mathrm{mm}$ it is somewhat too weak.

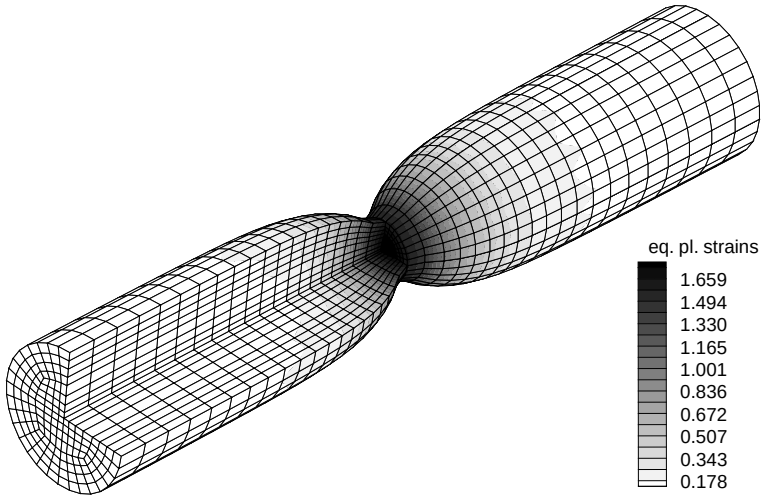

Fig. 6.2. Necking of a circular bar. Equivalent plastic strain at $w = 7\,\mathrm{mm}$

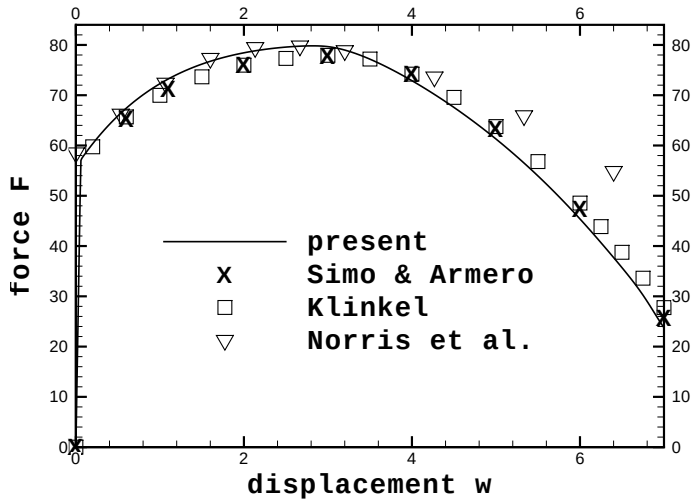

Fig. 6.3. Necking of a circular bar. Computational and experimental results of applied force F [kN] versus axial elongation w [mm]

6.2 Punching of a Conical Shell

In the second example of isotropic elastoplasticity we consider a conical shell subject to a constant ring load $\bar{\lambda}\, p$ with $p = 1\,\mathrm{GPa\,cm}$, see KLINKEL [20] and references therein. The material data as well as the system with the finite element discretization are depicted in Fig. 6.4. One quarter of the shell is discretized with $8 \times 8 \times 1$ elements. We use the von Mises yield criterion (29) along with isotropic hardening $\hat{\xi}(e^p) = he^p + (Y^\infty - Y^0)(1 - \exp(-\delta e^p))$.

In our computations we apply an arc-length method, where the vertical displacement w of the upper edge is controlled. Note that the shell exhibits two different stability points during the deformation process, namely at $w = 0.02\,\mathrm{cm}$ at the onset of a local rolling of the upper rim, whereas at $w = 1.21\,\mathrm{cm}$ a global snap through of the entire structure is observed, see Figs. 6.5 and 6.6. To avoid *zero-energy-modes* which can occur in applications of the EAS method, we use for the integration of the element stiffness matrix 9 instead of 8 Gauss points, which was firstly proposed by SIMO et al. [34]. The difference can be observed in Fig. 6.6, where the load-displacement curves considerably deviate from one another. Remarkably, the results of the proposed multiplicative model and those obtained by a theory based on generalized stress-strain measures for parameter $m = 0$, which leads to logarithmic stresses and strains, are in very good agreement. For details of the latter formulation, we refer to SCHRÖDER et al. [31]. In this context see also XIAO et al. [42]. The correspondence of the results might shed new light from the numerical side onto a controversial discussion about different competing plasticity models: those, based on the multiplicative decomposition, and others based on the additive framework.

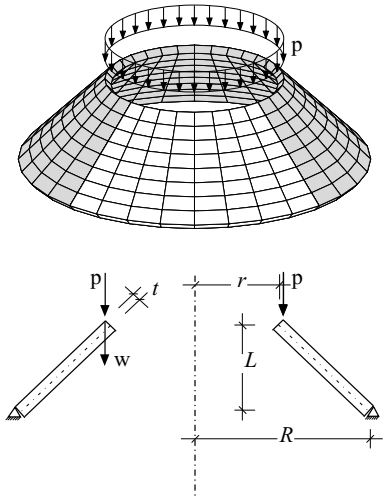

a)

Elasticity constants:
$E = 206.9\,\mathrm{GPa}\ ,\ \nu = 0.29$

Yield parameters:
$Y^0 = 0.45\,\mathrm{GPa}\ ,\ Y^\infty = 0.715\,\mathrm{GPa}$
$h = 0.12924\,\mathrm{GPa}\ ,\ \delta = 16.93$

Geometry:
$r = 1\,\mathrm{cm}\ ,\ R = 2\,\mathrm{cm}$
$L = 1\,\mathrm{cm}\ ,\ t = 0.1\,\mathrm{cm}$

b)

Fig. 6.4. Punching of a conical shell. (**a**) Geometry and finite element mesh. (**b**) Elastoplastic material and geometrical data

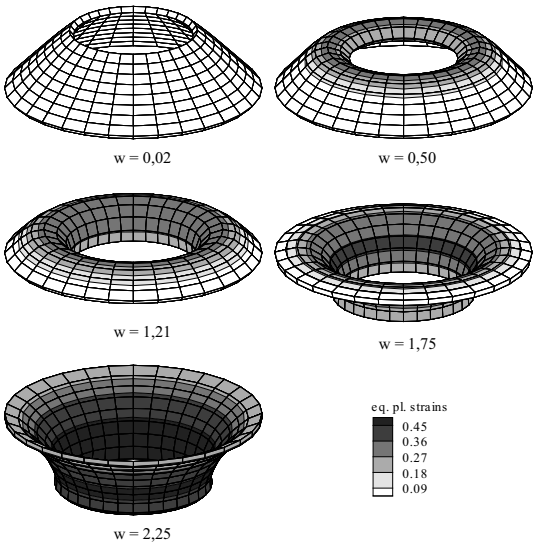

Fig. 6.5. Punching of a conical shell. Equivalent plastic strain on deformed structures at different stages of the punching process

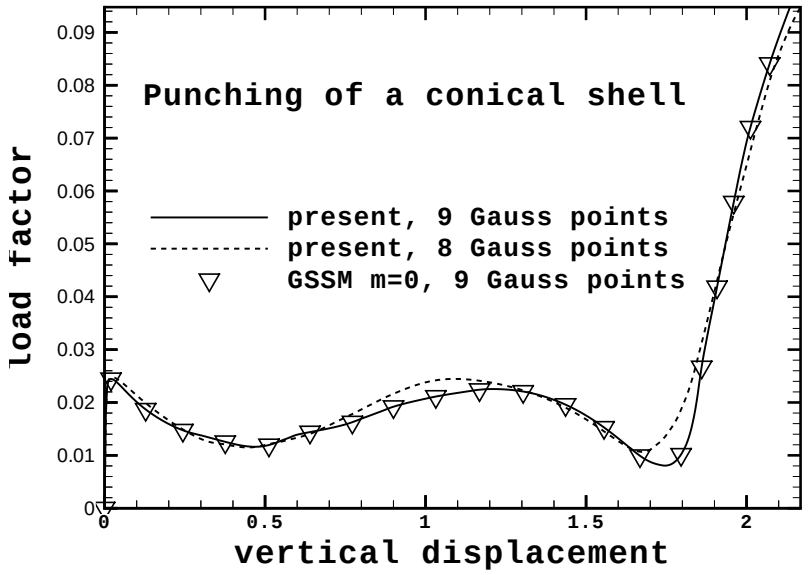

Fig. 6.6. Punching of a conical shell. Comparison of load-deflection curves. Multiplicative model (present) with 8 and 9 Gauss points versus generalized stress-strain measures (GSSM) for $m = 0$ with 9 Gauss points, [31]

6.3 Drawing of a Circular Blank

A circular blank of radius $R = 40\,\text{cm}$ and thickness $t = 1\,\text{cm}$ with a concentric hole of radius $R_i = 20\,\text{cm}$ is deep-drawn into a cup. In order to simulate the drawing process without using contact elements, the inner rim is uniformly pulled inwards in radial direction up to a maximum displacement of $\Delta u_r = 10\,\text{cm}$, while the outer rim is free. We choose plane stress conditions for our simplified model. The material is assumed to be isotropic in elasticity ($\mu = 80.19$ GPa and $\lambda = 110.74$ GPa) but orthotropic in its yield properties. The x- and y-axes of the coordinate system in Fig. 6.7 coincide with the axes of orthotropy. Two different materials are considered for orthotropic yielding. For material A the shear stresses dominate in the yield criterion, we set $Y_{xy} = 0.5 \cdot Y_{xx}/\sqrt{3}$. In contrast to A, for material B the normal stresses are predominant in yielding: for the shear yield stress we choose $Y_{xy} = 2.0 \cdot Y_{xx}/\sqrt{3}$ which is twice the isotropic value. For both materials $Y_{xx} = Y_{yy} = 0.45$ GPa holds.

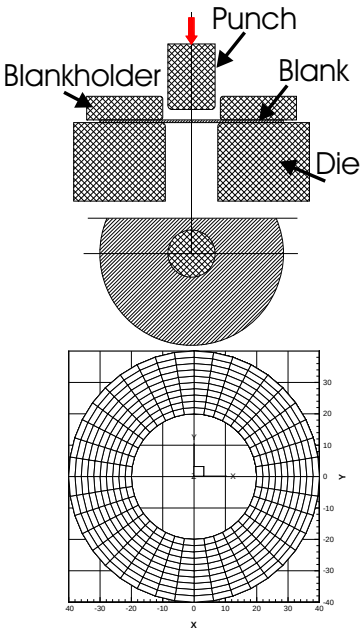

Fig.6.7. Real problem and its 2-dimensional model

As observed in deep-drawing experiments of rolled sheet metal the outer rim of the sheet exhibits waviness called *earing* owing to the anisotropy of the plastic material behaviour. As expected the plastic strains concentrate for material A at a 45° angle in the (x,y)-plane and for material B along the x- and y-axes, see Fig. 6.8 a), b).

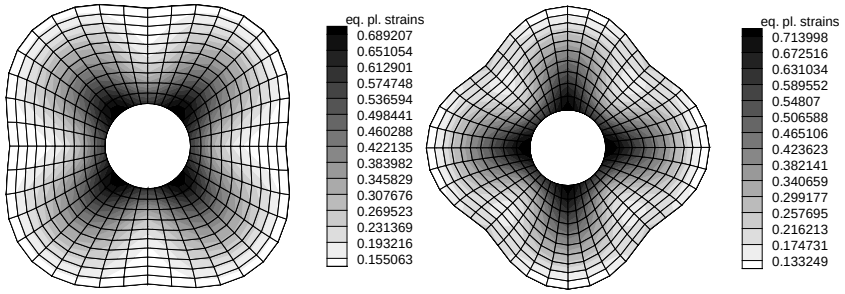

a) b)

Fig.6.8. Drawing of a circular blank. Modelling according to Papadopoulos & Lu [27]. Equivalent plastic strain on deformed structures at $\Delta u_r = 10\,\text{cm}$. (**a**) Material A: $Y_{xy} = 0.5 \cdot Y_{xy|isotropic}$. (**b**) Material B: $Y_{xy} = 2.0 \cdot Y_{xy|isotropic}$.

6.4 Simply Supported Circular Plate with Uniform Load

We now consider the elastoplastic deformation of a circular plate under dead load. The plate is simply supported in the z-direction at the bottom of the edges so that horizontal displacements and rotations at the edges may occur. Figure 6.9 a) depicts the geometry of the problem and its finite-element discretization. With respect to symmetry only one quarter of the plate is discretized. The mesh is chosen with one element through the thickness and 192 elements in plane for each quadrant. Again, two different materials, A and B are investigated, which both coincide in isotropic elasticity, but differ in the parameters of orthotropic plastic yielding, see Fig. 6.9 b).

Figure 6.10 depicts the load deflection curves where the load factor $\bar{\lambda}$ in $p_z(\bar{\lambda}) = \bar{\lambda}\, p_{z0}$ is plotted as a function of the vertical displacement of the center point of the circular plate. Again, we note a good agreement between the proposed model and that of the generalized stress-strain measures for $m = 0$. The deflection of the plate at the load levels $\bar{\lambda} = 400$ for material A and $\bar{\lambda} = 600$ for material B is shown in Fig. 6.11. As expected the plastic strains concentrate for material A at a 45° angle in the (x,y)-plane and for material B along the x- and y-axes. For a qualitative comparison see the deep-drawn cup in the centre of Fig. 6.11, taken from Raabe [28]. Our finite element simulation renders physically correct results concerning loci and number of the ears.

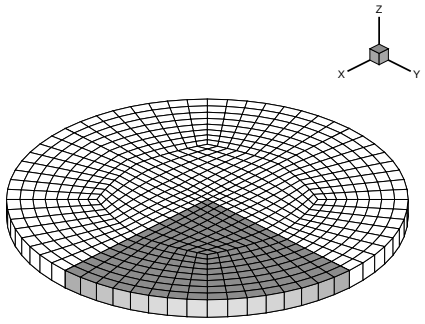

a)

Material parameters A & B:
$\lambda = 110.74\,\mathrm{GPa}\ ,\ \mu = 80.19\,\mathrm{GPa}$
$Y^0_{xx} = Y^0_{yy} = Y^0_{zz} = 0.45\,\mathrm{GPa}$
$Y^0_{xy} = Y^0_{xz} = Y^0_{yz}$
Material A: $Y^0_{xy} = 0.5 \cdot Y^0_{xx}/\sqrt{3}$
Material B: $Y^0_{xy} = 2.0 \cdot Y^0_{xx}/\sqrt{3}$

Geometry:
$R = 10\,\mathrm{cm}\ ,\ t = 1\ \mathrm{cm}$

Dead load:
$p_z = \bar{\lambda}\, p_{z0}\ ,\ p_{z0} = 10^{-4}\,\mathrm{GPa}$

b)

Fig. 6.9. Simply supported circular plate with uniform dead load. (**a**) Geometry and finite element mesh. (**b**) Material, geometrical and load data.

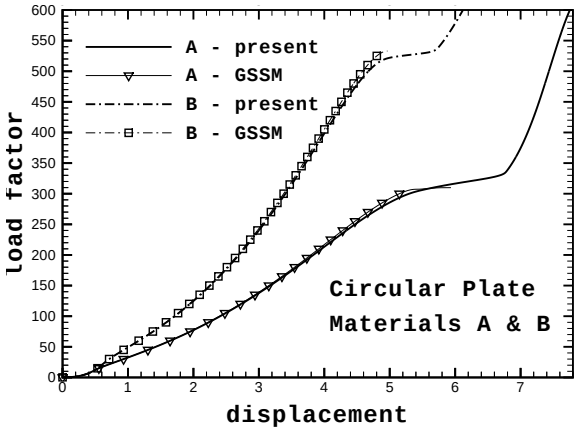

Fig. 6.10. Simply supported circular plate. Load displacement curves for materials A and B. Muliplicative model (present) versus generalized stress strain measures for $m = 0$ (GSSM)

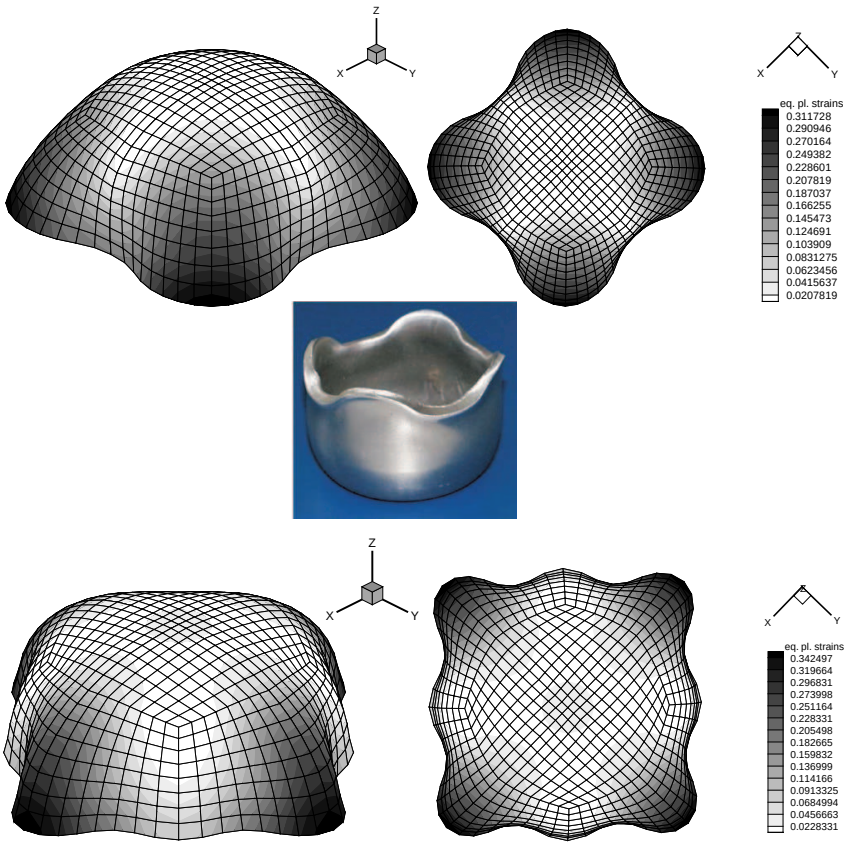

Fig. 6.11. Circular Plate. Equivalent plastic strain on deformed structures from perspective and bird's-eye view for material A at $\bar{\lambda} = 400$ (above), for material B at $\bar{\lambda} = 600$ (below). *Earing* at a deep-drawn cup (centre), [28]

7 Conclusions

In this paper a multiplicative formulation of orthotropic elastoplasticity at finite inelastic strains is presented and aspects of its finite element implementation are addressed. The governing constitutive equations, formulated in an invariant setting by the introduction of structural tensors, are formulated relative to the intermediate configuration. The yield function is expressed in terms of the symmetric part of the Mandel stresses and the associated back stresses. Kinematic as well as isotropic hardening are considered. A general return algorithm along with an exponential map is applied, the latter fulfills plastic incompressibility exactly. Representative numerical examples demonstrate the robustness of our solution algorithms and the predictive capacity of our finite element simulations to capture anisotropic phenomena such as *'earing'*. For the case of isotropy good agreement with computational results from the literature is achieved. Future research will concentrate on the evolution of anisotropy due to plastic deformations.

References

1. Bathe K.-J., Dvorkin E.N. (1984) A continuum mechanics based four node shell element for general nonlinear analysis. Eng Comput 1:77–88
2. Besdo D. (1981) Zur Formulierung von Stoffgesetzen der Plastomechanik im Dehnungsraum nach Ilyushin's Postulat. Ing-Arch 51:1–8
3. Betsch P., Gruttmann F., Stein E. (1996) A 4-node finite shell element for the implementation of general hyperelastic 3D-elasticity at finite strains. Comput Methods Appl Mech Eng 30:57–79
4. Betsch P., Stein E. (1996) An assumed strain approach avoiding artificial thickness straining for a nonlinear 4-node shell element. Commun Numer Methods Eng 11:899–910
5. Betten J. (1987) Formulation of anisotropic constitutive equations. In: Boehler J.P.(Ed.) Applications of tensor functions in solid mechanics, CISM Course No. 292. Springer, Heidelberg, 227–250
6. Bischoff M., Ramm E. (1997) Shear deformable shell elements for large strains and rotations. Int J Numer Methods Eng 40:4427–4449
7. Boehler J.P. (1987) Introduction to the invariant formulation of anisotropic constitutive equations. In: Boehler J. P.(Ed.) Applications of Tensor Functions in Solid Mechanics, CISM Course No. 292. Springer, Heidelberg, 13–30
8. de Borst R., Feenstra P.H. (1990) Studies in anisotropic plasticity with reference to the Hill criterion. Int J Numer Methods Eng 29:315–336
9. Casey J., Naghdi P. (1980) A remark on the use of the decomposition $\mathbf{F} = \mathbf{F}_e\mathbf{F}_p$ in plasticity. J Appl Mech 47:672–675
10. Casey J., Naghdi P. (1981) A correct definition of elastic and plastic deformation and its computational significance. J Appl Mech 48:983–985
11. Eidel B., Gruttmann F. (2002) On the formulation and finite element implementation of anisotropic multiplicative finite strain elastoplasticity. submitted to: PAMM, Proc Appl Math Mech

12. Eidel B., Gruttmann F. (2001) Finite strain inelasticity for isotropy, a simple and efficient finite element formulation. PAMM, Proc Appl Math Mech 1/1:185–186
13. Green A.E., Naghdi P.M. (1971) Some remarks on elastic-plastic deformations at finite strains. Int J Engin Sci 9:1219–1229
14. Gruttmann F., Eidel B. (2001) On the implementation of finite elastoplasticity using Almansi strain tensors and exact fulfillment of plastic incompressibility. IfS Preprint [J01-01].
15. Gruttmann F., Eidel, B. (2002) On the implementation of anisotropic finite strain plasticity. In: Mang H.A., Rammerstorfer F.G., Eberhardsteiner J. (Eds.) Proceedings of the Fifth World Congress on Computational Mechanics (WCCM V), July 7-12, 2002. Vienna University of Technology, Vienna, ISBN 3-9501554-0-6, `http://wccm.tuwien.ac.at`
16. Gruttmann F., Klinkel S., Wagner W. (1995) A finite rotation shell theory with application to composite structures. Rev Eur Élém Finis 4:597–631
17. Hackl K. (1997) Generalized standard media and variational principles in classical and finite strain elastoplasticity. J Mech Phys Solids 5:667–688
18. Hill R. (1948) A theory of the yielding and plastic flow of anisotropic metals. Proc R Soc Lond, Ser A 193:281–297
19. Klinkel S., Wagner W. (1997) An effective geometrically nonlinear brick element based on the EAS-method. Int J Numer Methods Eng 40:4529–4545
20. Klinkel S. (2000) Theorie und Numerik eines Volumen-Schalen-Elementes bei finiten elastischen und plastischen Verzerrungen. PhD Thesis, Universität Karlsruhe
21. Lubliner J. (1990) Plasticity theory, 1st edn. Macmillan Publishing Company, New York
22. Miehe C., Stein E. (1992) A canonical model of multiplicative elasto-plasticity: formulation and aspects of the numerical implementation. Eur J Mech, A/Solids 11:25–43
23. Miehe C. (1996) Exponential map algorithm for stress updates in anisotropic multiplicative elastoplasticity for single crystals. Int J Numer Methods Eng 39:3367–3390
24. Miehe C. (1998) A constitutive frame of elastoplasticity at large strains based on the notion of a plastic metric. Int J Solids Struct 35:3859–3897
25. Neff, P. (2002) Some results concerning the mathematical treatment of finite multiplicative elasto-plasticity. This volume
26. Norris D. M., Moran B., Scudder J. K., Quiñones D. F. (1978) A computer simulation of the tension test. J Mech Phys Solids 26:1–19
27. Papadopoulos P., Lu J. (2001) On the formulation and numerical solution of problems in anisotropic finite plasticity. Comput Methods Appl Mech Eng 190:4889–4910
28. Raabe R.D. (2002) Simulation und Experiment eines Näpfchenziehversuchs. `http://www2.mpie-duesseldorf.mpg.de/msu-web/Mitarbeiter/raabe/3`
29. Ramm E., Bischoff M., Braun M. (1994) Higher order nonlinear shell formulations – a step back into three dimensions. In: Bell K. (Ed.) From finite elements to the troll platform, Dept. of Structural Engineering, Norwegian Institute of Technology, Trondheim, 65–88
30. Sansour C., Kollmann F.G. (1998) Large viscoplastic deformations of shells. Theory and finite element formulation. Comput Mech 21:512–525

31. Schröder J., Gruttmann F., Löblein J. (2002) A simple orthotropic finite elastoplasticity model based on generalized stress-strain measures. Comput Mech, accepted for publication
32. Simó J.C. (1992) Algorithms for static and dynamic multiplicative plasticity that preserve the classical return mapping schemes of the infinitesimal theory. Comput Methods Appl Mech Eng 99:61–112
33. Simó J.C., Armero F. (1992) Geometrically non-linear enhanced strain mixed methods and the method of incompatible modes. Int J Numer Methods Eng 33:1413–1449
34. Simó J.C., Armero F., Taylor R.L. (1993) Improved version of assumed enhanced strain trilinear elements for 3D finite deformation problems. Comput Methods Appl Mech Eng 110:359–386
35. Simó J.C., Hughes T.J.R. (1998) Computational Inelasticity, 1st edn. Springer, New York
36. Smith G.F., Smith M.M., Rivlin R.S. (1963) Integrity basis for a symmetric tensor and a vector. The crystal classes. Arch Ration Mech Anal 12:93–133
37. Spencer A.J.M. (1971) Theory of invariants. In: Eringen A.C. (Ed.) Continuum Physics Vol. 1, Academic Press, New York. 239–353
38. Taylor R.L. (2000) FEAP - A Finite Element Analysis Program : Users Manual, University of California, Berkeley, `http://www.ce.berkeley.edu/rlt`
39. Tsakmakis Ch. (2002) Description of plastic anisotropy effects at large deformations. Part I: Restrictions imposed by the second law and the postulate of Il'iushin. Int J Plast, accepted for publication
40. Wagner W., Klinkel S., Gruttmann F. (2002) Elastic and plastic analysis of thin-walled structures using improved hexahedral elements. Comput Struct 80:857-869
41. Wriggers P., Eberlein R., Reese S. (1996) A comparison of three-dimensional continuum and shell elements for finite plasticity. Int J Solids Struct 33:3309–3326
42. Xiao H., Bruhns O.T., Meyers A. (2000) A consistent finite elastoplasticity theory combining additive and multiplicative decomposition of the stretching and the deformation gradient. Int J Plast 16:143–177